Distributions Mn oxidation states in grassland soils and their relationships with soil pores

Alexandra N Kravchenko[1]*, Jocelyn A Richardson[2], Jin Ho Lee[1], Andrey K Guber[1]

[1] Department of Plant, Soil and Microbial Sciences, Michigan State University, East Lansing, MI, United States,

[2] SLAC National Accelerator Laboratory, Stanford Synchrotron Radiation Lightsource, Menlo Park, 94025, USA

***Corresponding Author:**

Department of Plant, Soil and Microbial Sciences, Michigan State University, East Lansing, MI, 48824, United States.

E-mail: kravche1@msu.edu

Graphical summary

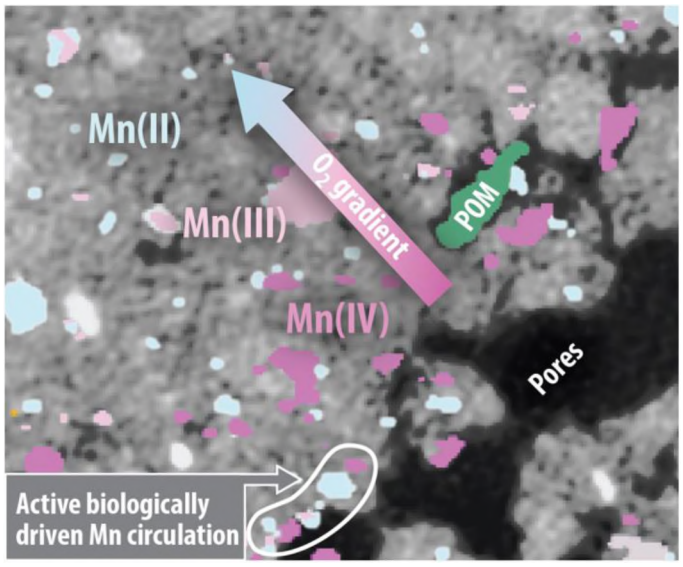

16 **Abstract**

17 Manganese (Mn) is a known active contributor to processing and cycling of soil organic
18 carbon (C), yet the exact mechanisms behind its interactions with C are poorly understood. Plant
19 diversity in terrestrial ecosystems drives feedback links between plant C inputs and soil pores,
20 where the latter, in turn, impact redox environment and Mn. This study examined associations
21 between soil pores (>36 μm Ø) and Mn within intact soils from two grassland ecosystems, after
22 their >6-year implementation in a replicated field experiment. We used μ-XRF imaging and
23 XANES spectroscopy to explore spatial distribution patterns of Mn oxidation states, combining
24 that with X-ray computed microtomography and 2D zymography. High plant diversity system
25 (restored prairie) increased soil C and modified spatial distribution patterns of soil pores as
26 compared to a single species system (monoculture switchgrass). In switchgrass the abundance of
27 oxidized and reduced Mn oxidation states varied with distance from pores consistently with
28 anticipated O_2 diffusion, while in the soil from restored prairie the spatial patterns suggested that
29 biological activity played a greater role in influencing Mn distributions. Based on the findings we
30 propose a hypothesis that Mn transformations promote C gains in soils of high plant diversity
31 grasslands.

32

33 **Key words:** soil organic C, plant diversity, soil pore architecture, X-ray computed micro-
34 tomography, micro-XRF imaging, XANES spectroscopy

35 **Synopsis:** Associations between micro-scale patterns in Mn oxidation states and soil pores
36 suggest positive contribution of Mn-transformation to carbon gains in soils of polyculture
37 grasslands.

38

INTRODUCTION

Soil organic carbon (C) drives soil fertility and mediates atmospheric CO_2 levels [1, 2]. Despite being extensively studied [3-5], the specific mechanisms involved in processing and protection of soil organic matter (SOM) remain enigmatic [6], preventing development of effective strategies in facilitating soil C gains. Recently, manganese (Mn) has been identified as an active contributor to abiotic and biological oxidation mechanisms of SOM processing and residue decomposition [7-11]. However, complex chemical and mineralogical behavior of Mn[12, 13] has thus far limited understanding, quantification, and modeling of Mn contribution to SOM protection and/or destabilization [13].

Mn facilitates SOM decomposition through its involvement in production of oxidative enzymes, such as Mn-peroxidase [14, 15] and through enhancement of the activity of other oxidative enzymes, such as peroxidases and laccases [16]. Moreover, many microbial decomposers have the capacity to oxidize Mn(II) in order to subsequently benefit from the decomposing power of reactive Mn(III) complexes [17, 18]. Yet, besides catalyzing decomposition, Mn also enables C protection. Dissolved organic C absorbs on surfaces of Mn oxides [19-21], often resulting in Mn nodules with C content several times exceeding that of the bulk soil [22, 23]. Mn(III)/Mn(IV) oxides coat surfaces of soil mineral particles, often trapping or coprecipitating with soil organic compounds [21, 24]. However, the permanence of SOM protection within Mn nodules is dubious, since in anaerobic conditions Mn(III)/Mn(IV) oxides can be reduced and dissolved though a number of abiotic and biotic pathways, often freeing the previously protected SOM [13].

The strong dependence of Mn oxidation state (OxS) on O_2 availability and microbial activity, as well as differences in Mn(II), Mn(III), and Mn(IV) solubilities, lead to formation of

62 complex spatial patterns in Mn distribution at spatial scales ranging from a few mm to entire soil
63 profiles. In anaerobic conditions, soluble Mn(II) formed during Mn oxide reduction diffuses
64 towards boundaries of oxic/anoxic transition zones, where it is then oxidized forming of
65 MnIII/MnIV nodules [22, 25, 26]. Fluctuating hydromorphic conditions and periodic exposure to oxic
66 environments leads to the formation of sizeable (> few mm) Mn(III)/Mn(IV) concretions,
67 orthsteins, and nodules [23, 27-30]. Moreover, the speed in the onset of oxic conditions defines the
68 particular shape of the resultant Mn concretions [31]. At fine (few cm) scales, spatial patterns in
69 Mn oxide depositions can reflect the transition zone's position, the availability of organic
70 materials subject to active microbial decomposition, and locations of hyphae from fungal
71 decomposers [10, 11, 32].

72 One of the drivers in the formation of active Mn cycling microsites in well-drained soils
73 are properties and locations of soil pores, a.k.a. soil pore architecture, which define the
74 microenvironments of microbial habitation [33, 34], generate local gradients in water and redox
75 potentials [35, 36], and local gradients in microbial activity [37, 38]. Characterization of soil pore
76 architecture via X-ray computed micro-tomography (μCT) enables quantifying the capacity for
77 O_2 supply from the atmosphere to move into the soil matrix via pores. The μCT-based data on
78 soil pore architecture can effectively predict the magnitude of O_2-sensitive soil processes, e.g.,
79 denitrification [39-41]. We hypothesize that soil pore architecture also affects the magnitude and
80 spatial patterns in Mn occurrence and OxSs, as well as involvement of Mn in soil C processing.
81 By combining μCT images with synchrotron X-ray Fluorescence (μ-XRF) imaging and X-ray
82 Absorption Near Edge Structure (XANES) spectroscopy it is possible to assess the role of pore
83 architecture in creating optimal environmental conditions for Mn-dependent oxidation and
84 reduction.

Many measurements of soil biological activity require sizeable (at least 20-50 mg) samples, which are taken from homogenized soil without a reference to their original positions within the soil matrix and surroundings. The traditional sampling approach prohibits learning about micro-environmental influences on biological processes [42]. Combining biological and chemical information from a range of data sources obtained from intact soil, including microscopy, spectrometry and spectroscopy images, and μCT, is a promising route for overcoming this problem [43, 44]. The method of 2D soil zymography is a tool for micro-scale *in-situ* mapping of extracellular enzyme activities that can be implemented efficiently and quickly across few to tens cm soil areas [45, 46]; thus, can identify hotspots of microbial activities [47-49]. Combined with μCT imaging, 2D zymography mapping has been used for exploring spatial patterns in enzyme activities and soil pore architecture [50] and for relating them to microbial activity [51]. In this study we will combine μCT imaging and 2D zymography with μ-XRF maps of Mn and its OxSs to jointly explore physical, biological, and chemical characteristics of potential relevance to soil C cycling.

It should be noted that contribution of Mn to residue decomposition and C cycling has been studied primarily in forest soils, where greater exchangeable Mn concentrations in litter and soils were often found to translate into faster litter decomposition [52, 53] and into lower C storage [54]. Whether Mn abundance has similar detrimental effect on C storage in soils of grasslands and arable lands is not known, therefore limiting the development of new strategies for promoting soil C gains via managing soil Mn. There are indications that the role of Mn in non-forest soils may differ from what is commonly observed in the forests. For example, nitrogen (N) additions to forest soils, e.g., N fertilization and N deposition, reduce Mn in plants [55] and lead to lower soil Mn [16, 56]. While in grasslands N additions increase extractable soil Mn [57].

Here we specifically focused on Mn in soils with long-term (>100 y) arable and then grassland history. High plant diversity is known to be one of the leading drivers of soil C gains [58]. Thus, for this study we selected vegetation systems of contrasting plant diversity, namely, a polyculture (>18 species) restored prairie and a monoculture (single species) switchgrass (*Panicum virgatum* L.) established on former intensively tilled agricultural land. The studied soils are well drained and coarse-textured (sandy loam), with pervasive oxic conditions and minimal oxic/anoxic gradients. Thus, the studied soil systems herein can be regarded as an end-member environment, i.e. the most oxic, for Mn studies.

The goal of the study is to explore the spatial distribution of Mn with different oxidation states within intact soils from grassland vegetation systems of contrasting plant diversity and to elucidate the drivers of the observed Mn spatial patterns. We specifically focused on exploring the influences of three factors expected to affect Mn OxS, namely: (i) medium-large (>36 μm Ø) soil pores, which serve as O_2 influx routes; (ii) soil particulate organic matter (POM) fragments within the soil matrix, which can act as hot-spots of microbial activity, thus influencing O_2 consumption and biological Mn transformations; and (iii) activity of extracellular enzymes, specifically, β-glucosidase, indicative of past root presence and past/current microbial activity.

METHODS

Soil sampling. Soil samples for bulk Mn and soil organic C (SOC) characterization were collected from 5 experimental sites of the Marginal Land Experiment from the Great Lake Bioenergy Research Center, established in 2013 along a North-South spatial gradient in Michigan and Wisconsin, USA (Supplement Figure S1). The soils of the sites belong to Alfisol, Spodosol, and Entisol types (https://lter.kbs.msu.edu/docs/glbrc/mle-site-histories.pdf). Prior to

131 the experiment establishment, all studied sites were in conventional row-crop agriculture or
132 pastures for at least several decades, and prior to European settlement they were under a variety
133 of forests, typical to North Central Midwest, including oak, hickory and white pine. At each site
134 a randomized complete block design experiment with 3-4 replications was set up. Two
135 undisturbed grassland systems of contrasting plant diversity were used in this study: monoculture
136 switchgrass (*Panicum virgatum* L., variety Cave-in-rock) and restored prairie, the system with 18
137 species of forbs, grasses and legumes also including switchgrass. Soil sampling of all replicated
138 plots of the two plant systems of all 5 sites was conducted in November-December 2019. At each
139 plot intact soil cores (Ø 5 cm) and loose soil adjacent to the cores were collected from 5-10 cm
140 depth. Soil cores were collected into plastic sleeves inserted into metal cylinders, which were
141 carefully driven into the soil. Immediately upon collection the samples were placed in foil wraps
142 and plastic bags to prevent drying (Supplement Figure S2). Prior to further analyses the samples
143 were stored at 4°C, the temperature consistent with the soil temperature during sampling, to
144 minimize disturbance to microbial activity. Loose soil samples, ground and 2-mm sieved, from
145 all studied sites were used for SOC, plant-available Mn, pH, and soil texture measurements.
146 Due to extremely cost- and time-consuming nature of the analyses, μCT imaging, 2D
147 zymography, μXRF imaging and XANES spectroscopy measurements were conducted only at
148 one of the five experimental sites (Lux Arbor), located at Kellogg Biological Station, Michigan
149 (85°19″ W, 42°26″ N). The soil of the site is well-drained mixed, mesic Typic Hapludalf
150 (Kalamazoo/Oshtemo series) formed on glacial outwash. Eight cores (2.5 cm in height), 4 from
151 each plant system of Lux Arbor site, were used in this study.
152 **Bulk soil analyses and characteristics**. Soil organic C was measured by combustion
153 analysis on Costech Analytical Elemental Combustion System model 4010 for CHNS-O

154 elemental analysis and Nitrogen / Protein determination (Costech Analytical Techologies, USA).
155 Plant-available Mn was determined by the 0.1 M hydrochloric acid extraction [59], and soil pH was
156 measured in a 1:5 soil to water ratio. Soil texture was measured using hydrometer method [60].
157 Across the studied sites, pH was equal to 5.9±0.1 in prairie and 6.0±0.1 in switchgrass soil
158 (p=0.27); in the Lux Arbor site the prairie and switchgrass pH values were equal to 6.4±0.2 and
159 6.2±0.2, respectively. The soils ranged in their texture from sand to sandy loam. The soil of Lux
160 Arbor site had 52% and 51% sand contents and 40% and 38% silt contents in its prairie and
161 switchgrass soil plots, respectively (p=0.88).

162 **Zymography.** Prior to μ-XRF imaging and XANES spectroscopy, β-glucosidase activity
163 was measured on the surface of each soil core using Time-Lapse-Zymography (TLZ) approach
164 [61] (Supplement Figure S3). Briefly, a hydrophilic polyamide membrane filter of 100 μm
165 thickness and pore size of 0.45 μm (Tao Yuan, China) was saturated in 6 mM solution of the of
166 4-methylumbelliferyl-β-D-glucopyranoside (Sigma-Aldrich, Inc., St. Louis, MO, U.S.A.) and
167 placed on the soil surface. The membrane was photographed every minute in UV light during a
168 45 min incubation on the soil surface. Obtained images were converted to 4-methylumbelliferone
169 (MUF, i.e., the product of enzyme catalytical reaction) content maps, using the calibration curve
170 obtained for the standard MUF solutions in the same camera and light setting. The β-glucosidase
171 activity was calculated in each pixel of the membrane (18 x 18 μm) as a largest time derivative
172 of MUF content time series, corrected for MUF losses due to diffusion from enzymatically active
173 spots to the soil matrix. Calculated spatial distributions of β-glucosidase activity on the soil
174 surfaces are referred further to as 2D zymography maps.

175 **X-ray μCT scanning and image analyses.** Soil cores were scanned using a North Star
176 Imaging X3000 X-ray μCT system (Rogers, USA) housed at Michigan State University. Prior to

177 scanning, the cores were drained at -28 kPa and then μCT scanned at a resolution of 18.2 μm
178 with energy settings of 75 keV and 450 μA and 3014 projections. The X-ray μCT images were
179 reconstructed using efX software (North Star, Rogers, USA). Image analyses were performed in
180 ImageJ (v1.5) software [62]. Image preprocessing consisted of a 3D Median filtering (two-voxel
181 radius in all directions) and contrast enhancement (0.6% saturated pixel setting). The processed
182 images were segmented into pores and solids using Otsu method, as implemented in ImageJ;
183 pores identified on the segmented images will be referred to as visible pores. The scanning
184 resolution and image processing used in the study allowed us to reliably visualize pores with Ø
185 >36 μm. Particulate organic matter (POM) was identified using a machine-learning algorithm
186 from image analysis software package *ilastic* [63], with gray values of the image, their 1st
187 derivative and 2nd derivative (texture information) in 3D used POM identification. Distance to
188 the nearest pore and to the nearest POM fragment (Supplement Figure S4) was determined for
189 each solid image voxel by using 3D distance transformation tool of ImageJ. For each soil sample
190 we reported the following μCT-based characteristics: image-based porosity (the volume of the
191 visible pores expressed as the percent of the total soil volume), distance to pores, and distance to
192 POM. The latter two characteristics were obtained as the average distances between individual
193 voxels which do not belong to pores or POM and the border of the nearest visible (Ø >36 μm)
194 pore or the nearest POM fragment.

195 **XRF imaging and XANES spectroscopy.** Synchrotron μXRF imaging and XANES
196 spectroscopy at the Mn K-edge were performed at beamline 7-2 (large format XRF imaging
197 beamline) at the Stanford Synchrotron Radiation Lightsource (SSRL), SLAC National
198 Accelerator Laboratory. A water-cooled double crystal Si (111) monochromator was energy
199 calibrated using the first derivative of a Mn metal foil to 6537.7 eV [64]. Beamline 7-2 is equipped

200 with a four element silicon drift detector (Hitachi). Capillary focusing optics provided a spot size
201 of either 100 or ~35 μm depending on the size of the mapping area (total Mn or Mn oxidation,
202 respectively). Soil cores were first mounted in a 3D printed frame and covered with a 6 μm thick
203 perforated XRF film (SpectroMembrane® Mylar® Thin-Film, Chemplex Industries, Inc., Palm
204 City, Florida, USA) in order for the cross-sectional core face to remain upright in the X-ray
205 beam during analysis. The soil cores and frame were then mounted onto polycarbonate holders.
206 Each soil cross-section was imaged above the Mn K-edge (6700 eV) at a coarse resolution (100
207 μm step size) to provide maps of total Mn abundance on the soil surfaces.
208 Total Mn images combined with zymography and μCT scans were then used to
209 determine regions of interest for Mn multi-energy mapping and XANES spectroscopy, in order
210 to generate images of Mn oxidation (Supplement Figure S3). Multi-energy maps were collected
211 at various energies around the Mn K-edge (6553, 6559, 6562 and 6564 eV) at higher resolution
212 (35 μm) on smaller regions of interest. Principal component analysis (PCA) and simplex volume
213 maximization [65] (both types of cluster analysis) performed using the Microanalysis Toolkit [66] at
214 the beamline provided the best estimates of locations to perform XANES spectroscopy in order
215 to determine the variability in Mn chemistry present in a given mapped region. XANES spectra
216 were background subtracted and normalized using the Athena package [67]. End-member XANES
217 spectra that correspond to the most different Mn chemistry were determined by performing a
218 PCA in SIXPACK [68], and were verified by a linear combination fitting of previously published
219 standards[64] in Athena. To create maps of an individual OxS of Mn, a least-squared fitting of the
220 end-member spectra (corresponding to Mn(II), Mn(III) and Mn(IV)) were applied to the multi-
221 energy maps in SMAK (Supplement Figure S5).

Image analyses of Mn spatial patterns. To enable comparisons of Mn distributions, in every oxidation map we identified the locations with the highest abundance (top 5th percentile) of each of the three Mn OxSs ((Mn(II), Mn(III), and Mn(IV)). Selecting the top 5th percentile provided a balance between the ability to focus on high abundance of a particular Mn OxS and to obtain sufficiently large areas of that OxS for meaningful exploration of the spatial patterns. Then we focused on the spatial patterns in distributions of the individual OxSs, i.e., the locations where only one of the three studied Mn OxS was in the top 5th percentile, and of the two OxSs combinations, i.e., the locations where two of the three studied Mn OxS were in the top 5th percentile (Supplement Figure S6). The sizes of locations where all three OxSs were in high abundance were very small to negligible, thus their spatial distribution patterns could not be reliably assessed.

Mn oxidation state distribution hypothesis: We hypothesize that the micro-scale spatial distribution patterns of Mn oxidation and oxidation combinations result from combined contributions of Mn present in a solid form, e.g., as Mn holding minerals or oxides [10, 69] and in a mobile form, e.g., as soluble Mn(II) or chelated Mn(III) [70]. We further hypothesize that, given transient nature of soil pores and their relatively fast turnover [71], it is the mobile forms of Mn(II) and Mn(III) and the recently formed Mn(III) and Mn(IV) oxide solid forms that will primarily respond to pore structure and to redox distributions resultant from the pore structure. While Mn associated with inherent soil minerals will be randomly distributed through the soil matrix. The specific expectations regarding the spatial patterns in distributions of the individual OxSs that will be affected by the spatial patterns in distribution of soil pores, are as follows:

1) The associations between areas of high abundance of Mn(II) and soil pores will be driven by mobile Mn(II), while high Mn(II) abundance spots representing Mn-containing minerals will not contribute to relationships with pores. High Mn(II) abundance locations associated with pores thus are assumed to be the places dominated by mobile Mn(II) and to correspond to either reduced conditions or to locations of active microbial Mn processing.

2) The locations with high abundance of Mn(III), where it is not co-located with either Mn(II) or Mn(IV), are assumed to be the places where Mn(III) is present in a mobile chelated form or in a newly formed solid oxide form[10], and correspond to either locations of active microbial Mn processing or a very recent onset of oxidized conditions.

3) The locations with high Mn(IV), when not accompanied by either high Mn(II) or Mn(III) abundances, are assumed to be the places of solid highly oxidized Mn.

Of specific interest are the following combinations (i.e. co-location) of Mn OxSs:

1) Mn(II) and Mn(III), hypothesized to reflect the locations of active biologically-driven use of Mn for decomposition or of to/from reduction/oxidation transition, referred to further on as Mn(II-III), and

2) Mn(III) and Mn(IV), as the combination hypothesized to correspond to a recent onset of oxidized conditions and/or completion of active fungal-driven Mn oxidation, referred to as Mn(III-IV). In addition,

3) Mn(II) and Mn(IV) combination, assumed to represent the locations with either the fastest onset of oxidation or an onset of anoxic reduced conditions, referred to as Mn(II-IV).

For each sample we determined the fraction of the total studied soil surface with high abundance of the individual OxSs and their combinations, referred to further on as areas of high abundance. To explore colocations between Mn abundance and β-glucosidase we determined the fraction of the soil surface with non-negligible β-glucosidase activity that corresponded to high abundance of Mn individual OxSs or OxS combinations. Then, to enable comparisons among the samples, we further standardized it by the fraction of the total soil surface with non-negligible β-glucosidase activity.

We explored the distribution of high abundance of individual Mn OxSs and OxS combinations as a function of distances from the pores and distances from POM fragments in the soils of the two studied plant systems. For that, the maps of the listed above high abundances of individual OxSs and combinations of OxSs were overlayed with the distance-to-pores or distance-to-POM maps of μCT images in ImageJ. We considered 20 distance classes, ranging from 1 to 20 pixels from the pores/POM. For each distance class we determined the total area of the soil surface belonging to the class and then the fraction of that area occupied by the studied Mn OxSs or OxS combinations. In order to facilitate comparisons among the samples these fractions were further standardized by the total area occupied by the particular Mn OxS/combination of OxSs within the sample, these are further referred to as relative abundances.

Statistical analyses. Comparisons between the two studied systems in terms of soil plant-available Mn, soil organic C, other loose soil measurements, e.g., pH and texture, as well as areas with high abundance of individual Mn OxSs and OxS combinations were conducted using the mixed model approach [72]. The data were fitted with statistical models (as specified below), followed by checking the model assumptions, and by the system comparisons.

For bulk plant-available Mn and soil C we used the data from all five experimental sites; and the statistical model for the analysis included the fixed effect of the plant system, along with random effects of sites and of experimental field blocks nested within the sites. Statistical models for comparing the two plant systems in terms of areas with high abundances of Mn OxSs and OxS combinations in the samples from Lux Arbor site consisted of the fixed effect of the plant system and random effect of blocks. Normality of the residuals and equal variance assumptions were checked using normal probability plots and side-by-side box plots. When found violated, e.g., in case of soil organic C, the data were transformed using either square root- or log-transformation. The results of the system comparisons are reported as statistically significant at $p<0.05$ or as trends at $p<0.1$. Function *lmer* from R l*me4* package was used for fitting statistical models, with comparisons between the means conducted using *emmeans* package.

The relationships between high abundance of individual OxSs and OxS combinations with distances to pores or to POM fragments were fitted with cubic linear regression equations. Cubic regression was chosen to allow flexibility in addressing a range of patterns in shapes of the relationships yet had relatively few model parameters. Function *lm* of R was used for the regression analysis.

RESULTS

Soil and pore characteristics. Across the 5 studied experimental sites, soil plant-available Mn was significantly higher in prairie than in monoculture switchgrass (Fig. 1a), the trend that was consistently present in all sites (Supplement Fig. S7). SOC was also higher in prairie than in switchgrass (Fig. 1b). Soil data from the Lux Arbor site followed the same pattern

310 of differences between prairie and switchgrass systems as the rest of the sites (red-circled data
311 points on Fig. 1a and 1b).

312 Total image-based porosities (volumetric fraction of pores > 36 μm Ø in the total soil
313 volume) in the studied samples were similar in prairie and switchgrass soils (Fig. 1c) and tended
314 to be numerically, but not statistically significantly, higher in switchgrass than in prairie soils.
315 The average distance to pores was greater in switchgrass (~470 μm), as compared to prairie
316 (~340 μm) (Fig. 1d). Approximately 34% of the total soil solid voxels were located at >500 μm
317 distances from the visible pores in the switchgrass samples, while only 17% in the prairie.
318 Approximately 10% and 17% of the soil solid voxels were at <100 μm distance from the nearest
319 pore in switchgrass and prairie soils, respectively. The maximum observed distances to pores
320 were equal to 1300 μm and 1700 μm for prairie and switchgrass systems, respectively.

321 POM fragments occupied 0.5% and 0.8% of the total soil volume in prairie and
322 switchgrass soil samples, and did not differ between the two systems ($p=0.4$). The average
323 distance from POM tended to be shorter in prairie samples, 1000 μm, than in switchgrass
324 samples, 1600 μm ($p<0.1$).

325 The two systems did not differ in terms of β-glucosidase activity. Enzymatically active
326 areas occupied 5.1% and 4.8% of the total studied area in prairie and switchgrass soil samples,
327 respectively, and their average activities within the enzymatically active areas were equal to 7.9
328 and 9.6 pmol min^{-1} mm^{-2} (with standard error of 0.8).
329

Figure 1. Averages and standard errors (error bars) for plant-available Mn (0.1 M hydrochloric acid extraction [59]) (a) and soil organic carbon (b) from 5 experimental sites; and for image-based porosity (i.e., pores with >36 µm Ø) (c) and distances to pores (d) obtained from X-ray µCT images of the soil cores from Lux Arbor, MI site. Stars mark significant differences between the two plant systems ($p<0.05$). Dots represent individual data points from all sites, the data points from the Lux Arbor experimental site on (a) and (b) are marked by red circles. Black circle marks the outlier that was not used in the statistical analysis of the image-based porosity data.

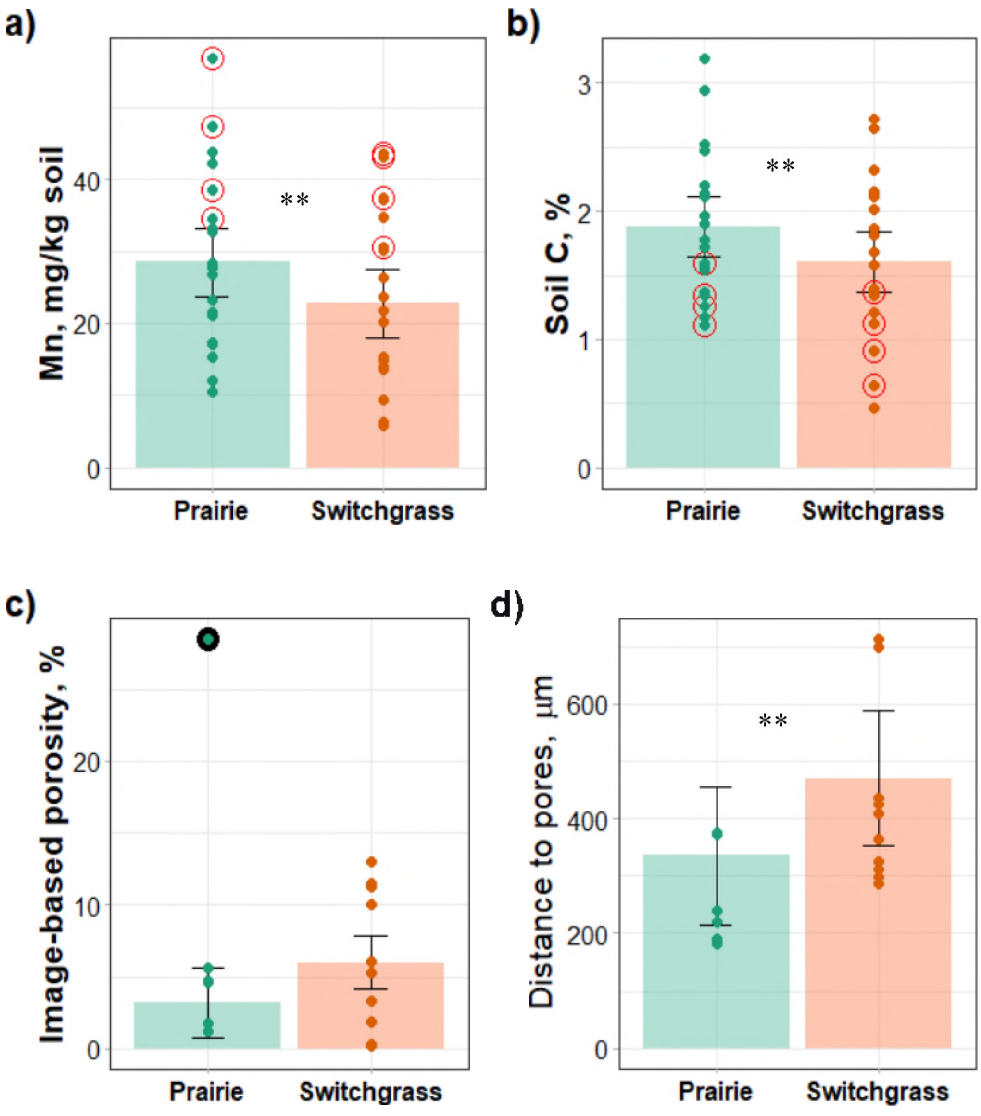

Areas with high abundance of Mn oxidation states. Plant system had no effect on the abundances of Mn(II) and Mn(IV), but locations with high abundance of Mn(III) occupied almost twice the space in the switchgrass as in the prairie soil (Fig. 2a). Areas of high Mn(II-III) and Mn(II-IV) also were greater in switchgrass, while the areas with high Mn(III-IV) were >10 times greater in soils of prairie than switchgrass system (Fig. 2b).

Abundances of the studied Mn OxSs were generally not related to the locations with high β-glucosidase activity. Also, there were no differences in Mn co-located with the enzymes between the two systems for most of Mn OxSs (Supplement Figure S8). One exception was Mn(III-IV): the area occupied by Mn(III-IV) colocated with β-glucosidase was higher in the switchgrass than in prairie soil ($p<0.1$) (Supplement Figure S8b).

Distribution of Mn oxidation states as a function of distance from pores and POM. The relationships between the studied Mn OxSs and distances to pores were fitted with cubic regression models for each plant system (Supplement Table 1 and Supplement Fig. S9a). Fitted regression lines (and their confidence intervals) for the individual OxSs or OxS combinations that were statistically significantly associated with the distance from pores in at least one of the two plant systems are shown on Fig. 3. Distance to pores was associated with Mn(II-III) and Mn(III-IV) in both prairie and switchgrass, while it was associated with Mn(II) and Mn(II-IV) only in the soil from the switchgrass system (Supplement Table 1).

Figure 2. Areas of high abundance (5th percentile) Mn oxidation states (OxS) in the soils from prairie and switchgrass systems, either dominated by just a single OxS (a), or with simultaneously high abundance of two OxSs (b). Stars mark significant differences between the two plant systems ($p<0.05$).

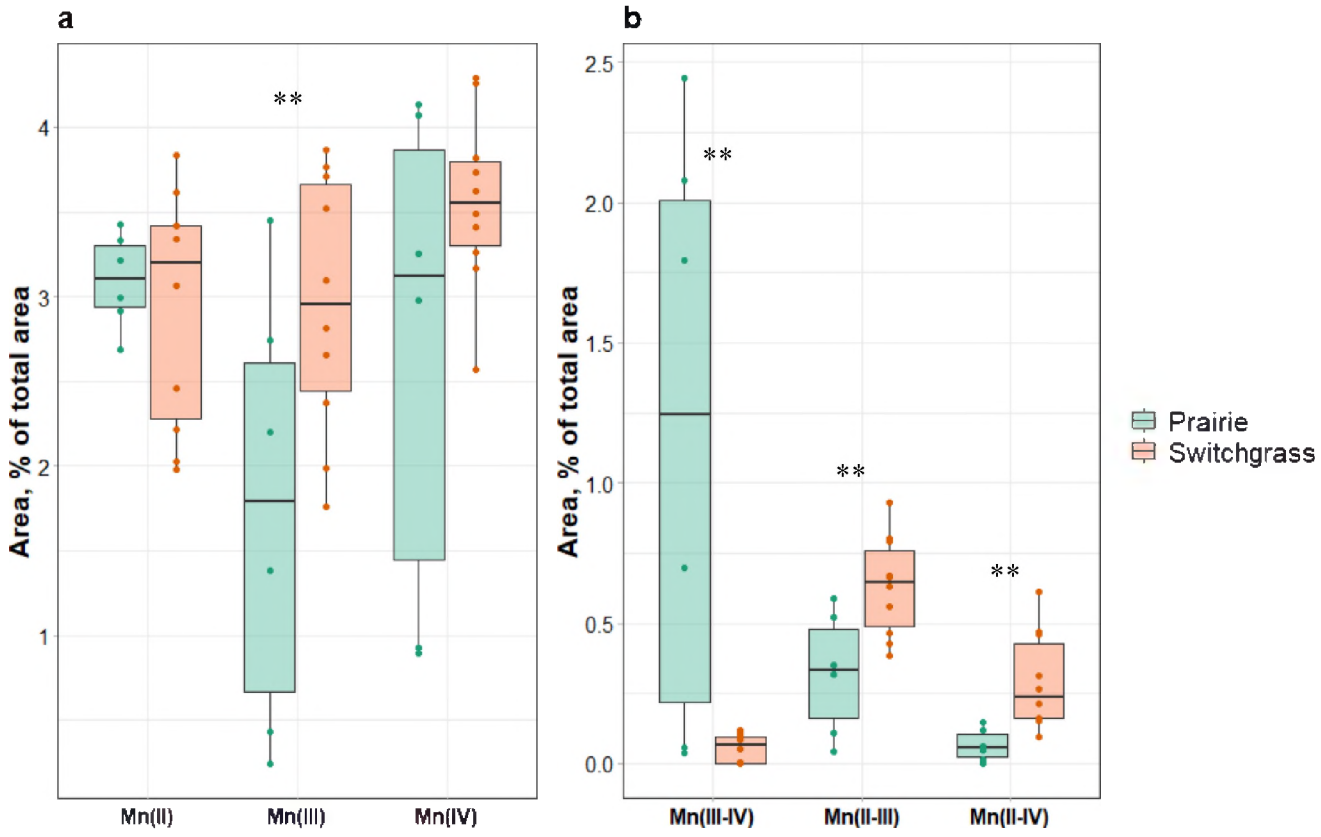

365 Several common trends in Mn OxSs distribution as a function of distance to pores were
366 observed in both plant systems (Figs. 3a and 3b). The abundance of areas with high Mn(II-III)
367 and Mn(III-IV) was the greatest at 150-400 μm distances from pores and the lowest < 100 μm
368 and > 500 μm distances from pores. Across both systems, the trend in abundances of co-located
369 two OxSs was: Mn(II-IV) (closest) < Mn(III-IV) < Mn(II-III) (farthest) (Figs. 3a and 3b).
370 Specifically, for Mn(II-IV) the peaks of the highest abundance were located at 30 and 130 μm
371 distances from pores in prairie and switchgrass, respectively, for Mn(III-IV) the peaks were at
372 165 and 210 μm, and for Mn(II-III) the peaks were at 220 and 410 μm (Supplement Table 2).
373 Distances to pores did not influence the areas with high abundance of individual Mn(III) and
374 Mn(IV) OxSs.
375 Relative abundance of Mn(II) tended to decrease in the soil matrix with an increasing
376 distance to pores in the prairie soil (Fig. 3a), while it increased as a function of distance in the
377 switchgrass ($p<0.1$) (Fig. 3b). While the peak distances from pores to Mn(III-IV) and Mn(II-III)
378 were very close to each other in the prairie system, at 165 and 220 μm, respectively (Fig. 3a,
379 Supplement Table 2), Mn(III-IV) was closer to pores (210 μm) than Mn(II-III) (410 μm) in
380 monoculture switchgrass (Fig. 3b, Supplement Table 2). The peak of Mn(II-IV) was almost in
381 the immediate vicinity of the pores (Fig. 3a) in prairie (30 μm, Supplement Table 2), while in
382 switchgrass the peak of Mn(II-IV) was located at 130 μm distance from the pores (Fig. 3b,
383 Supplement Table 2).
384 Fitted regression lines with their confidence intervals for the individual OxSs or OxS
385 combinations that were significantly associated with the distance from POM in at least one of the
386 two systems are shown on Figs. 3c and 3d (p-values from regression fitting can be found in
387 Supplement Table 1 and fitted regressions plotted along with the data are in Supplement Fig.

388 S9b). Only Mn(III) was associated with the distance from POM in both plant systems (yet, only
389 at $p<0.1$ in prairie). The peak of Mn(III) abundance was observed at distances of ~750 and 650
390 μm from POM in prairie and switchgrass, respectively (Figs. 3c and 3d). In the switchgrass
391 system, Mn(IV) and Mn(II-III) were also significantly associated with the distance from POM,
392 with maximum abundances also at ~650 μm distance.
393
394 **DISCUSSION**
395 The micro-scale spatial distribution of Mn OxSs in the studied grassland soils was
396 associated with distances from soil pores in a manner consistent with our hypothesized roles of
397 mobile and solid Mn OxSs. The distributions in the polyculture restored prairie differed from
398 those in the monoculture switchgrass in a manner suggestive that SOC gains observed during the
399 past > 6 years in the prairie could be associated with a greater proliferation of aerobic conditions
400 within the soil matrix and subsequent Mn transformations. This finding is important to
401 understanding the development of soil microsites primed for Mn redox reactions contributing to
402 plant matter decomposition and SOM storage.
403

Figure 3. Cubic regression models fitted to the relative abundances of individual Mn OxSs and OxS combinations data vs. distance to pores for soils from prairie (a) and switchgrass (b) plant systems and vs. distance to particulate organic matter fragments (POM) for soils from prairie (c) and switchgrass (d) plant systems. Gray ribbons mark 95% confidence intervals for the regression mean predictions. Vertical lines mark approximate positions of the highest relative abundances for the observed Mn oxidation states (OxS) with values reported in Supplement Table 2. Examples of X-ray μCT images overlayed with maps of selected Mn OxSs/ OxS combinations are shown in (e).

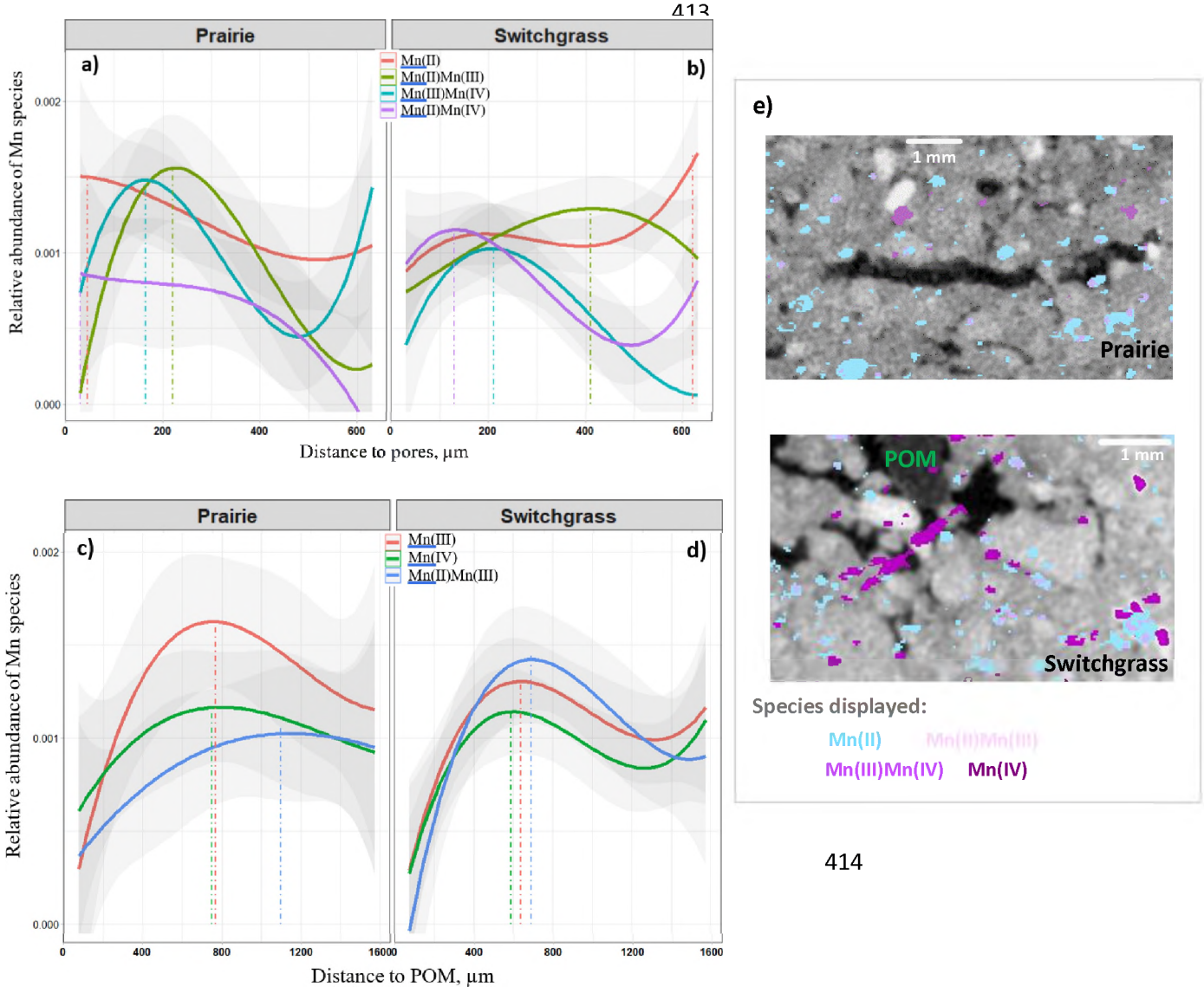

418

419 **General trends in Mn spatial distribution patterns.** Contrasting vegetation diversity
420 patterns, e.g., monoculture switchgrass vs. diverse prairie vegetation, are known to affect
421 properties and spatial arrangement of soil pores [73]. Larger distances to > 36 μm Ø pores observed
422 in the soils of switchgrass system as compared to the prairie (Fig. 1d) imply that larger volumes
423 within its soil matrix can potentially become anoxic. These pores, according to the Young-
424 Laplace equation, are drained at a capillary pressure > 8.2 kPa, which is less than the soil field
425 capacity (33 kPa). Therefore, in most soils these pores retain water only during very short
426 periods of time (2-4 hours), immediately after irrigation or heavy rainfall events, while most of
427 the time they act as air conduits. The shorter distances to > 36 μm Ø pores observed in the prairie
428 system's soil suggest that the soil volumes affected by O_2 shortages were smaller, and that
429 aerobic conditions were more common and wider spread, as compared to switchgrass soil. O_2
430 diffuses from large air-filled pores into the surrounding fine pores, while mobile Mn(II) and
431 partly mobile Mn(III), stabilized by organic ligands[70], diffuse in pore solutions from anaerobic
432 areas towards the oxic zone. Mn oxidation takes place at the locations where the partial pressure
433 of O_2 is just sufficient for Mn oxidation [74]. The peak abundance of co-located Mn(III-IV) in both
434 prairie and switchgrass soil systems was preferentially observed at ~180-200 μm distances from
435 the pores (Figs. 3a and 3b). Thus, it can be surmised that the zone separating Mn
436 oxidation/reduction conditions in the studied soils is located at ~180-200 μm distance from >36
437 μm Ø pores. This observation aligns with the results of our previous study, which demonstrated
438 that in these soils the volume of poorly aerated matrix affecting the N_2O emission and the N_2O
439 production via denitrification was best defined by an 180 μm distance from the pores [39].
440

441 Besides transition zones, Mn oxides (Mn(III-IV)) also can form in vicinity (at a few μm
442 to few mm distances) from fungal hyphae through reactions with organic acids and exopolymers
443 of fungal origin. This phenomenon, first noted almost 150 years ago (refs. in [75]), is observed
444 even after fungi cease their activity [76]. Since >36 μm Ø pores were likely the preferred habitat
445 for fungi [77, 78], it is possible that the Mn(III-IV) peaks at ~180-200 μm distances from pores also
446 reflect the presence of such organic compounds of fungal origin.
447
448 **Differences in Mn spatial distribution patterns between prairie and switchgrass**
449 **systems.** Despite a number of commonalities between the two systems, Mn spatial patterns were
450 substantially disparate, suggesting differences in prevailing processes, e.g., physical vs.
451 biological, driving Mn transformations in switchgrass vs. prairie soils. In switchgrass, the
452 greatest abundance of Mn(II-IV) and Mn(III-IV) were the closest to the pores, at 130 μm and
453 210 μm distances, respectively (Supplement Table 2). This was followed by the greatest
454 abundance of more reduced Mn(II-III) (at 410 μm), while the most reduced phase (Mn(II)) was
455 at its greatest abundance at 650 μm distance from the pores (Fig. 3b). Such pattern in spatial
456 distribution of Mn OxS is consistent with the general understanding of the roles of O_2 and Mn(II)
457 diffusion in Mn reduction and oxidation (Fig. 4). That is, Mn(II) in the switchgrass soil was
458 maximal in the reduced, low O_2 zone farthest from the large air-filled >36 μm pores. It was
459 probably located in smaller (<36 μm Ø) water-filled and O_2-depleted pores, and as it moved
460 towards the >36 μm pores it began oxidizing to Mn(III), as Mn(II-III), and upon further
461 approaching the oxic zone to Mn(III-IV) and Mn(II-IV) (Fig. 3b).
462 In comparison, the spatial pattern of Mn OxSs in the prairie soil appeared to be
463 contradictory to these general expectations of oxidation/diffusion drivers. First, in the prairie soil

464 Mn(II) was not associated with the distance and was numerically the highest in close proximity
465 to pores. Second, both more reduced Mn(II-III) and more oxidized Mn(III-IV) were at their
466 maxima at the same distance from pores (~200 µm) (Fig. 3a).
467

468 **Figure 4.** Schematic representation of the fluxes and processes involved in Mn transformation in
469 proximity to an air-filled soil pore. Red arrows and color represent O_2 fluxes and a relative extent
470 of the oxic zone within the soil matrix. Blue arrows and color represent diffusion of reduced
471 forms of Mn and the anoxic zone. Deposition of Mn oxides and active Mn bio-transformations
472 by soil microorganisms are maximal within the transition zone, which in the studied soils is
473 located at ~200 µm distances from the pores.

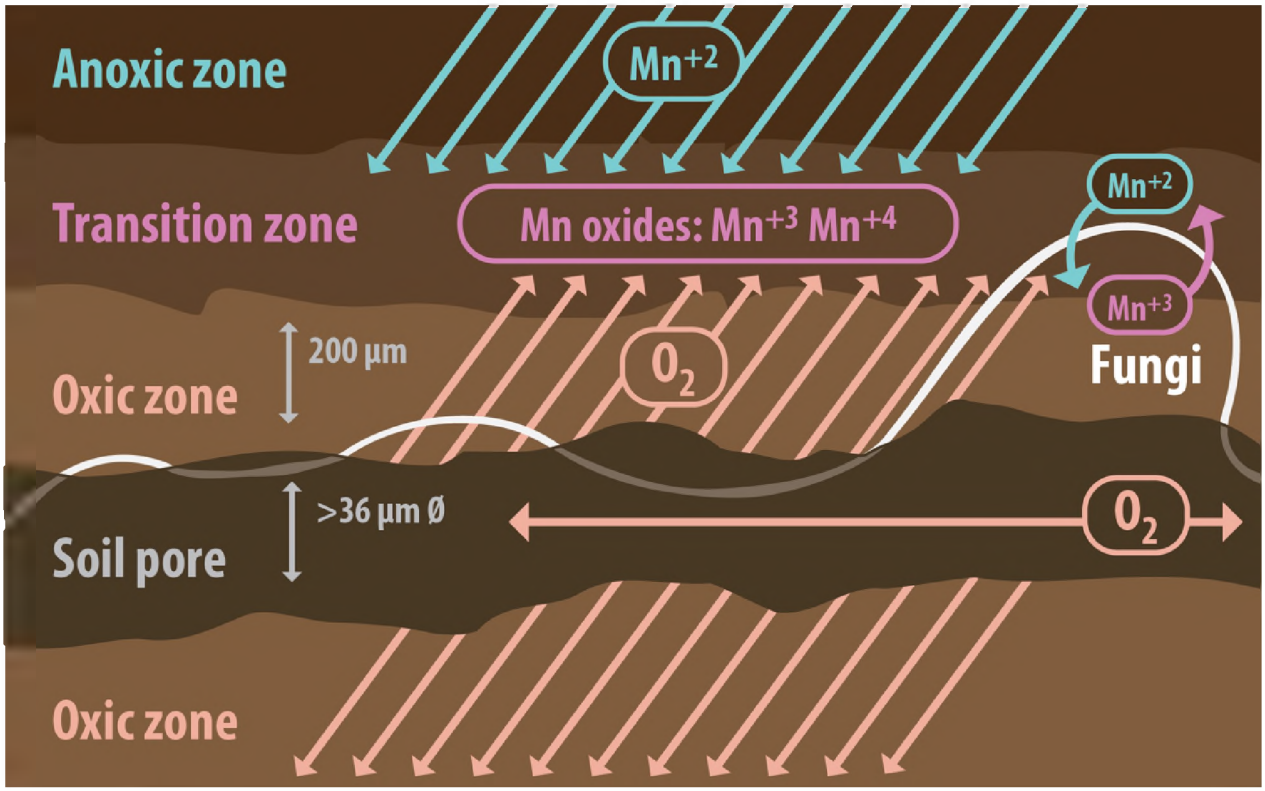

474 Moreover, higher plant-available Mn in the prairie soils across five studied sites (Fig. 1a),
475 was inconsistent with its better aeration status. Plant-available Mn, i.e., Mn extractable by weak

476 acids, mainly consists of soluble Mn(II) with some presence of Mn(III) [79]. Greater soil volumes
477 affected by anoxic conditions in switchgrass soil should have resulted in more Mn(II). Indeed,
478 there were greater areas occupied by more reduced Mn(II-IV) and Mn(II-III) OxS combinations
479 in switchgrass soil (Fig. 2b) consistent with an onset in reduction and dissolution of Mn(IV)
480 oxides in anaerobic conditions. Yet, still the prairie soil had higher extractable Mn.

481 These inconsistencies might be indicative of a more substantial involvement of microbes
482 in Mn transformations in prairie soils. For example, a possible reason for a lack of decrease in
483 Mn(II) in close proximity to pores could be the enhanced microbial activity in pore vicinities
484 involving biological Mn reduction. Microbes, especially fungi, are known to transform Mn(II) to
485 Mn(III) via oxidizing enzymes, including Mn peroxidase, as well as via O radical species [10, 11, 17,
486 74, 80]. The resultant Mn(III), often in a form of mobile Mn(III)–ligand complexes, can oxidize a
487 number of organic substrates, most notably lignin, while reducing back to Mn(II) [10, 11, 13, 17, 74].
488 Medium sized (30-150 μm Ø) pores and the soil near them serve as hotspots of microbial activity
489 [38, 50]. Active repeated cycling of Mn(II)-Mn(III) by microbes [11] can be the reason for the lack of
490 decreases in Mn(II) in proximity to the pores in the prairie soil and for the peak in abundance of
491 Mn(II-III) close to the pore boundaries (220 μm) there (Fig. 3a).

492 Soluble Mn(III) not involved in organic oxidation can disproportionate into Mn(II) and
493 Mn(IV) and precipitate as Mn(III-IV) oxides [80], which are often found in great quantities within
494 few mm to few cm oxic-anoxic transition zones [10, 74] as well as within nearby plant and fungal
495 residues [11, 81]. While the Mn(III-IV) peaks occurred at similar distances from pores (~200 μm) in
496 both soils of this study, suggesting a common influence from oxic/anoxic pore-driven spatial
497 patterns, the area occupied by high Mn(III-IV) was >10 times greater in prairie than in
498 switchgrass soil (Fig. 2b). Yet, the volume of the soil in close proximity to pores was only ~1.5

499 times higher in prairie (17%) than in switchgrass (10%) soil, thus could not be the only reason
500 for its much greater Mn(III-IV) abundance. Stronger and more widely distributed biological
501 activity involving Mn processing in prairie soil is what we hypothesize to be a contributor to
502 greater Mn(III-IV) formation. Measurements from a companion study indeed demonstrated
503 significantly higher microbial biomass in prairie than in switchgrass soil (Lee et al., in
504 preparation). Higher plant-available Mn observed in prairie soil (Fig. 1a) also could be related to
505 mobile Mn(II) or Mn(III)-complexes generated by enhanced biological activity and enhanced
506 dynamic Mn cycling by microorganisms. Production of Mn-based extracellular enzymes,
507 including but not limited to Mn peroxidase, by the microorganisms also might be contributing [15].
508 Activity of Mn-peroxidase exhibits hot-spot behavior [54] and thus can be responsible for some of
509 the observed spatial patterns in Mn distributions.
510 It is worth noting that a substantial influence of POM on spatial patterns of several Mn
511 OxSs and OxS combinations was observed in switchgrass soil, while almost none was present in
512 prairie (Supplement Table 1 and Figs. 3c and 3d). In addition, the colocation of Mn(III-IV) with
513 β-glucosidase was significantly higher in switchgrass than in prairie soil (Supplement Figure
514 S8b). These observations suggest that locations with high microbial activity, such as POM
515 fragments or spots marked by high enzyme activity, played an important role in Mn distribution
516 patterns of switchgrass soil. But their role was less pronounced, as compared to that of the
517 distance to pores, in the prairie soil. This could be an outcome of a contrasting soil aeration
518 regime of switchgrass soil, with greater anaerobic areas, that made the influence of microbial
519 activity hot-spots more noticeable. Widespread oxic conditions and potentially more widely
520 distributed biological activity of prairie soils might have made the influence of such hotspots on
521 Mn distribution less detectable.

Potential implications for mechanisms of soil C protection and future directions. Our findings support the notion that microenvironmental conditions play an important role in the biological processes involving Mn [10]. In previous studies with forest soils, areas with enhanced Mn(II) oxidation across the oxic–anoxic transition zone demonstrated the greatest potential to oxidize lignin and solubilize soil organic matter [10]. Greater abundance of such biologically driven Mn oxidation is regarded as one of the drivers of C losses in forest soils [16, 54, 82]. However, it appears that the negative effect of this process in soils of agricultural/grassland land use history is either negligible or is not leading to C losses. We speculate that intermediate products of SOM decomposition and microbial activity might not be fully decomposed to CO_2 in such soils, but protected within soil matrix, possibly, even within the newly formed Mn(III-IV) oxides, thus leading not to losses but gains in total soil C (Fig. 1b). Mn-oxides strongly absorb soil organic matter [19, 83, 84], especially when they are in a poorly crystalline phase shortly after their formation [81]. However, they are prone to reductive dissolution when the O_2 becomes deficient [83], releasing any sorbed organic matter. Our data suggest that, in polyculture restored prairie soils, microbial activity leads to Mn(III-IV) formation, accompanied by SOM incorporation and protection. Due to the pervasive nature of medium (>36 μm Ø) well-aerated pores through prairie soil, the onsets of anoxic conditions in such pores are infrequent and short, meaning that Mn(III-IV) oxides with adsorbed SOM remain intact and SOM remains protected. While further analyses are needed, this is a promising hypothesis to be tested on a potential additional mechanism of enhanced C storage in the soils with diverse prairie vegetation.

ACKNOWLEDGEMENTS

We would like to thank Maxwell Oerther for assistance with sample processing, Maxwell Oerther and Jenie Gil Lugo for assistance with sample collection, and Michelle Quigley for conducting X-ray μCT scanning of the samples. We are indebted to Chelsea Mamott for the artwork and for help with graphical abstract preparation.

This research was funded by the USDA-NIFA Program (Award# 2022-67019-36104), by the NSF LTER Program (DEB 1027253) at the Kellogg Biological Station, by the Great Lakes Bioenergy Research Center, U.S. Department of Energy, Office of Science, Office of Biological and Environmental Research under Award Number DE-SC0018409, and by Michigan State University AgBioResearch. Use of the Stanford Synchrotron Radiation Lightsource, SLAC National Accelerator Laboratory, is supported by the U.S. Department of Energy, Office of Science, Office of Basic Energy Sciences under Contract No. DE-AC02-76SF00515. The SSRL Structural Molecular Biology Program is supported by the DOE Office of Biological and Environmental Research, and by the National Institutes of Health, National Institute of General Medical Sciences (P30GM133894).

SUPPORTING INFORMATION

Supporting information contains 1) summaries and individual fits of cubic regression models fitted to μXRF Mn OxSs and distances to pores and POM data, 2) locations of experimental sites, 3) methodological illustrations of soil core sampling, distance to pore concept, XANES spectroscopy end-members, and Mn OxSs abundance image processing, 4) soil plant-available Mn and organic C data from individual experimental sites, and 5) relative abundances of Mn OxSs in relation to areas with non-negligible β-glucosidase activity.

References

1. Lal, R., Soil carbon sequestration impacts on global climate change and food security. *Science* **2004,** *304*, (5677), 1623-1627.
2. Lal, R.; Monger, C.; Nave, L.; Smith, P., The role of soil in regulation of climate (vol 376, 20210084, 2021). *Philos T R Soc B* **2021,** *376*, (1838).
3. Cotrufo, M. F.; Wallenstein, M. D.; Boot, C. M.; Denef, K.; Paul, E., The Microbial Efficiency-Matrix Stabilization (MEMS) framework integrates plant litter decomposition with soil organic matter stabilization: do labile plant inputs form stable soil organic matter? *Global Change Biol* **2013,** *19*, (4), 988-995.
4. Gunina, A.; Kuzyakov, Y., From energy to (soil organic) matter. *Global Change Biol* **2022**.
5. Kuzyakov, Y.; Subbotina, I.; Chen, H. Q.; Bogomolova, I.; Xu, X. L., Black carbon decomposition and incorporation into soil microbial biomass estimated by C-14 labeling. *Soil Biol Biochem* **2009,** *41*, (2), 210-219.
6. Craig, M. E.; Geyer, K. M.; Beidler, K. V.; Brzostek, E. R.; Frey, S. D.; Stuart Grandy, A.; Liang, C.; Phillips, R. P., Fast-decaying plant litter enhances soil carbon in temperate forests but not through microbial physiological traits. *Nat Commun* **2022,** *13*, (1), 1229.
7. Berg, B., Litter decomposition and organic matter turnover in northern forest soils. *Forest Ecology and Management* **2000,** *133*, (1-2), 13-22.
8. Berg, B.; Steffen, K. T.; McClaugherty, C., Litter decomposition rate is dependent on litter Mn concentrations. *Biogeochemistry* **2007,** *82*, (1), 29-39.
9. Davey, M. P.; Berg, B.; Emmett, B. A.; Rowland, P., Decomposition of oak leaf litter is related to initial litter Mn concentrations. *Canadian Journal of Botany-Revue Canadienne De Botanique* **2007,** *85*, (1), 16-24.
10. Jones, M. E.; Nico, P. S.; Ying, S.; Regier, T.; Thieme, J.; Keiluweit, M., Manganese-Driven Carbon Oxidation at Oxic-Anoxic Interfaces. *Environ Sci Technol* **2018,** *52*, (21), 12349-12357.
11. Keiluweit, M.; Nico, P.; Harmon, M. E.; Mao, J.; Pett-Ridge, J.; Kleber, M., Long-term litter decomposition controlled by manganese redox cycling. *Proceedings of the National Academy of Sciences of the United States of America* **2015,** *112*, (38), E5253-E5260.
12. Cragg, S. M.; Beckham, G. T.; Bruce, N. C.; Bugg, T. D. H.; Distel, D. L.; Dupree, P.; Etxabe, A. G.; Goodell, B. S.; Jellison, J.; McGeehan, J. E.; McQueen-Mason, S. J.; Schnorr, K.; Walton, P. H.; Watts, J. E. M.; Zimmer, M., Lignocellulose degradation mechanisms across the Tree of Life. *Current Opinion in Chemical Biology* **2015,** *29*, 108-119.
13. Li, H.; Santos, F.; Butler, K.; Herndon, E., A Critical Review on the Multiple Roles of Manganese in Stabilizing and Destabilizing Soil Organic Matter. *Environmental Science & Technology* **2021,** *55*, (18), 12136-12152.
14. Kadri, T.; Rouissi, T.; Brar, S. K.; Cledon, M.; Sarma, S.; Verma, M., Biodegradation of polycyclic aromatic hydrocarbons (PAHs) by fungal enzymes: A review. *Journal of Environmental Sciences* **2017,** *51*, 52-74.
15. Kranabetter, J. M., Increasing soil carbon content with declining soil manganese in temperate rainforests: is there a link to fungal Mn? *Soil Biol Biochem* **2019,** *128*, 179-181.
16. Whalen, E. D.; Smith, R. G.; Grandy, A. S.; Frey, S. D., Manganese limitation as a mechanism for reduced decomposition in soils under atmospheric nitrogen deposition. *Soil Biology & Biochemistry* **2018,** *127*, 252-263.
17. Hofrichter, M., Review: lignin conversion by manganese peroxidase (MnP). *Enzyme and Microbial Technology* **2002,** *30*, (4), 454-466.

18. Jones, M. E.; LaCroix, R. E.; Zeigler, J.; Ying, S. C.; Nico, P. S.; Keiluweit, M., Enzymes, Manganese, or Iron? Drivers of Oxidative Organic Matter Decomposition in Soils. *Environmental Science & Technology* **2020,** *54*, (21), 14114-14123.
19. Chorover, J.; Amistadi, M. K., Reaction of forest floor organic matter at goethite, birnessite and smectite surfaces. *Geochim Cosmochim Ac* **2001,** *65*, (1), 95-109.
20. Gu, B. H.; Schmitt, J.; Chen, Z. H.; Liang, L. Y.; McCarthy, J. F., ADSORPTION AND DESORPTION OF NATURAL ORGANIC-MATTER ON IRON-OXIDE - MECHANISMS AND MODELS. *Environmental Science & Technology* **1994,** *28*, (1), 38-46.
21. Stuckey, J. W.; Goodwin, C.; Wang, J.; Kaplan, L. A.; Vidal-Esquivel, P.; Beebe, T. P., Jr.; Sparks, D. L., Impacts of hydrous manganese oxide on the retention and lability of dissolved organic matter. *Geochemical Transactions* **2018,** *19*.
22. Rennert, T.; Haendel, M.; Hoeschen, C.; Lugmeier, J.; Steffens, M.; Totsche, K. U., A NanoSIMS study on the distribution of soil organic matter, iron and manganese in a nodule from a Stagnosol. *European Journal of Soil Science* **2014,** *65*, (5), 684-692.
23. Zaidelman, F. R.; Stepantsova, L. V.; Nikiforova, A. S.; Krasin, V. N.; Dautokov, I. M.; Krasina, T. V., Neoformations (Nodules and Placic Layers) in Surface-Gleyed Loamy Sandy Soils of the Northern Part of the Tambov Plain. *Eurasian Soil Sci+* **2019**, 494-506.
24. Estes, E. R.; Andeer, P. F.; Nordlund, D.; Wankel, S. D.; Hansel, C. M., Biogenic manganese oxides as reservoirs of organic carbon and proteins in terrestrial and marine environments. *Geobiology* **2017,** *15*, (1), 158-172.
25. Manceau, A.; Tamura, N.; Celestre, R. S.; MacDowell, A. A.; Geoffroy, N.; Sposito, G.; Padmore, H. A., Molecular-scale speciation of Zn and Ni in soil ferromanganese nodules from loess soils of the Mississippi Basin. *Environmental Science & Technology* **2003,** *37*, (1), 75-80.
26. Yu, X. L.; Fu, Y. N.; Brookes, P. C.; Lu, S. G., Insights into the Formation Process and Environmental Fingerprints of Iron-Manganese Nodules in Subtropical Soils of China. *Soil Science Society of America Journal* **2015,** *79*, (4), 1101-1114.
27. Patrick, W. H.; Delaune, R. D., CHARACTERIZATION OF OXIDIZED AND REDUCED ZONES IN FLOODED SOIL. *Soil Sci Soc Am Pro* **1972,** *36*, (4), 573-&.
28. Schwertmann, U.; Fanning, D. S., IRON-MANGANESE CONCRETIONS IN HYDROSEQUENCES OF SOILS IN LOESS IN BAVARIA. *Soil Science Society of America Journal* **1976,** *40*, (5), 731-738.
29. Sun, Z. X.; Jiang, Y. Y.; Wang, Q. B.; Owens, P. R., Fe-Mn nodules in a southern Indiana loess with a fragipan and their soil forming significance. *Geoderma* **2018,** *313*, 92-111.
30. Zaidelman, F. R.; Nikiforova, A. S.; Stepantsova, L. V.; Volokhina, V. P., Dark gray soils on two-layered deposits in the north of Tambov Plain: Agroecology, properties, and diagnostics. *Eurasian Soil Sci+* **2012,** *45*, (5), 459-471.
31. Blume, H. P., The mechanism of mottling and nodule formation in poorly drained soils Engl. sum. *Z Pflanzenernahr Bodenk* **1968,** *119*, ((2)), 124-134.
32. Pinzari, F.; Cuadros, J.; Migliore, M.; Napoli, R.; Najorka, J., Manganese translocation and concentration on Quercus cerris decomposing leaf and wood litter by an ascomycetous fungus: an active process with ecosystem consequences? *Fems Microbiol Ecol* **2018,** *94*, (8).
33. Xia, Q.; Rufty, T.; Shi, W., Soil microbial diversity and composition: Links to soil texture and associated properties. *Soil Biology and Biochemistry* **2020,** *149*, 107953.
34. Xia, Q.; Zheng, N.; Heitman, J. L.; Shi, W., Soil pore size distribution shaped not only compositions but also networks of the soil microbial community. *Appl Soil Ecol* **2022,** *170*, 104273.
35. Dorau, K.; Uteau, D.; Hovels, M. P.; Peth, S.; Mansfeldt, T., Soil aeration and redox potential as function of pore connectivity unravelled by X-ray microtomography imaging. *Eur J Soil Sci* **2021**.
36. Wanzek, T.; Keiluweit, M.; Varga, T.; Lindsley, A.; Nico, P. S.; Fendorf, S.; Kleber, M., The Ability of Soil Pore Network Metrics to Predict Redox Dynamics is Scale Dependent. *Soil Systems* **2018,** *2*, (4).

37. Nunan, N.; Ritz, K.; Rivers, M.; Feeney, D. S.; Young, I. M., Investigating microbial micro-habitat structure using X-ray computed tomography. *Geoderma* **2006,** *133*, (3-4), 398-407.
38. Nunan, N.; Wu, K. J.; Young, I. M.; Crawford, J. W.; Ritz, K., Spatial distribution of bacterial communities and their relationships with the micro-architecture of soil. *Fems Microbiology Ecology* **2003,** *44*, (2), 203-215.
39. Kravchenko, A. N.; Guber, A. K.; Quigley, M. Y.; Koestel, J.; Gandhi, H.; Ostrom, N. E., X-ray computed tomography to predict soil N2O production via bacterial denitrification and N2O emission from soils in contrasting bioenergy cropping systems. *Gcb Bioenergy* **2018**, 1-17.
40. Rohe, L.; Apelt, B.; Vogel, H. J.; Well, R.; Wu, G. M.; Schluter, S., Denitrification in soil as a function of oxygen availability at the microscale. *Biogeosciences* **2021,** *18*, (3), 1185-1201.
41. Schluter, S.; Zawallich, J.; Vogel, H. J.; Dorsch, P., Physical constraints for respiration in microbial hotspots in soil and their importance for denitrification. *Biogeosciences* **2019,** *16*, (18), 3665-3678.
42. Baveye, P. C.; Otten, W.; Kravchenko, A.; Balseiro-Romero, M.; Beckers, É.; Chalhoub, M.; Darnault, C.; Eickhorst, T.; Garnier, P.; Hapca, S.; Kiranyaz, S.; Monga, O.; Mueller, C. W.; Nunan, N.; Pot, V.; Schlüter, S.; Schmidt, H.; Vogel, H.-J., Emergent Properties of Microbial Activity in Heterogeneous Soil Microenvironments: Different Research Approaches Are Slowly Converging, Yet Major Challenges Remain. **2018,** *9*.
43. Lucas, M.; Pihlap, E.; Steffens, M.; Vetterlein, D.; Koegel-Knabner, I., Combination of Imaging Infrared Spectroscopy and X-ray Computed Microtomography for the Investigation of Bio- and Physicochemical Processes in Structured Soils. *Frontiers in Environmental Science* **2020,** *8*.
44. Schlueter, S.; Eickhorst, T.; Mueller, C. W., Correlative Imaging Reveals Holistic View of Soil Microenvironments. *Environmental Science & Technology* **2019,** *53*, (2), 829-837.
45. Guber, A.; Kraychenko, A.; Razavi, B. S.; Uteau, D.; Peth, S.; Blagodatskaya, E.; Kuzyakov, Y., Quantitative soil zymography: Mechanisms, processes of substrate and enzyme diffusion in porous media. *Soil Biology & Biochemistry* **2018,** *127*, 156-167.
46. Spohn, M.; Carminati, A.; Kuzyakov, Y., Soil zymography - A novel in situ method for mapping distribution of enzyme activity in soil. *Soil Biology & Biochemistry* **2013,** *58*, 275-280.
47. Bilyera, N.; Kuzyakova, I.; Guber, A.; Razavi, B. S.; Kuzyakov, Y., How "hot" are hotspots: Statistically localizing the high-activity areas on soil and rhizosphere images. **2020**.
48. Ma, X. M.; Razavi, B. S.; Holz, M.; Blagodatskaya, E.; Kuzyakov, Y., Warming increases hotspot areas of enzyme activity and shortens the duration of hot moments in the root-detritusphere. *Soil Biology & Biochemistry* **2017,** *107*, 226-233.
49. Zhang, X.; Dippold, M. A.; Kuzyakov, Y.; Razavi, B. S., Spatial pattern of enzyme activities depends on root exudate composition. *Soil Biology and Biochemistry* **2019,** *133*, 83-93.
50. Kravchenko, A. N.; Guber, A. K.; Razavi, B. S.; Koestel, J.; Blagodatskaya, E. V.; Kuzyakov, Y., Spatial patterns of extracellular enzymes: combining X-ray computed micro-tomography and 2D zymography. *Soil Biology & Biochemistry* **2019,** *135*, 411-419.
51. Kravchenko, A. N.; Guber, A. K.; Gunina, A.; Dippold, M.; Kuzyakov, Y., Pore-scale view of microbial turnover: combining 14C imaging, μCT, and zymography after adding soluble carbon to soil pores of specific sizes. *European Journal of Soil Science* **2020,** *doi.org/10.1111/ejss.13001*.
52. Sun, T.; Cui, Y.; Berg, B.; Zhang, Q.; Dong, L.; Wu, Z.; Zhang, L., A test of manganese effects on decomposition in forest and cropland sites. *Soil Biology & Biochemistry* **2019,** *129*, 178-183.
53. Trum, F.; Titeux, H.; Ponette, Q.; Berg, B., Influence of manganese on decomposition of common beech (Fagus sylvatica L.) leaf litter during field incubation. *Biogeochemistry* **2015,** *125*, (3), 349-358.
54. Kranabetter, J. M.; Philpott, T. J.; Dunn, D. E., Manganese limitations and the enhanced soil carbon sequestration of temperate rainforests. *Biogeochemistry* **2021,** *156*, (2), 195-209.

55. van Diepen, L. T.; Frey, S. D.; Sthultz, C. M.; Morrison, E. W.; Minocha, R.; Pringle, A., Changes in litter quality caused by simulated nitrogen deposition reinforce the N-induced suppression of litter decay. *Ecosphere* **2015,** *6*, (10), 1-16.
56. Swathi A., T.; Rakesh, M.; Premsai S., B.; Louis S., T.; William K., T.; Subhash C., M., Chronic N-amended soils exhibit an altered bacterial community structure in Harvard Forest, MA, USA. *FEMS Microbiology Ecology* **2013,** *83*, (2), 478-493.
57. Hou, S.-L.; Hattenschwiler, S.; Yang, J.-J.; Sistla, S.; Wei, H.-W.; Zhang, Z.-W.; Hu, Y.-Y.; Wang, R.-Z.; Cui, S.-Y.; Lu, X.-T.; Han, X.-G., Increasing rates of long-term nitrogen deposition consistently increased litter decomposition in a semi-arid grassland. *New Phytologist* **2021,** *229*, (1), 296-307.
58. Yang, Y.; Tilman, D.; Furey, G.; Lehman, C., Soil carbon sequestration accelerated by restoration of grassland biodiversity. *Nature Communications* **2019,** *10*, (1), 718.
59. Sorensen, R. C.; Oelsligle, D. D.; Knudsen, D., EXTRACTION OF ZN, FE, AND MN FROM SOILS WITH 0.1 N HYDROCHLORIC ACID AS AFFECTED BY SOIL PROPERTIES, SOLUTION - SOIL RATIO, AND LENGTH OF EXTRACTION PERIOD. *Soil Sci* **1971,** *111*, (6), 352-+.
60. Gee, G. W.; Or, D., Particle-size analysis. In *Methods of soil analysis. Part 4. Physical methods*, Agron. Monogr. 5. ASA and SSSA: Madison, WI, 2002; pp 255-294.
61. Guber, A.; Blagodatskaya, E.; Juyal, A.; Razavi, B. S.; Kuzyakov, Y.; Kravchenko, A., Time-lapse approach to correct deficiencies of 2D soil zymography. *Soil Biology and Biochemistry* **2021,** *157*, 108225.
62. Schindelin, J.; Arganda-Carreras, I.; Frise, E.; Kaynig, V.; Longair, M.; Pietzsch, T.; Preibisch, S.; Rueden, C.; Saalfeld, S.; Schmid, B.; Tinevez, J. Y.; White, D. J.; Hartenstein, V.; Eliceiri, K.; Tomancak, P.; Cardona, A., Fiji: an open-source platform for biological-image analysis. *Nat Methods* **2012,** *9*, (7), 676-682.
63. Berg, S.; Kutra, D.; Kroeger, T.; Straehle, C. N.; Kausler, B. X.; Haubold, C.; Schiegg, M.; Ales, J.; Beier, T.; Rudy, M.; Eren, K.; Cervantes, J. I.; Xu, B.; Beuttenmueller, F.; Wolny, A.; Zhang, C.; Koethe, U.; Hamprecht, F. A.; Kreshuk, A., ilastik: interactive machine learning for (bio)image analysis. *Nat Methods* **2019,** *16*, (12), 1226-1232.
64. Manceau, A.; Marcus, M. A.; Grangeon, S., Determination of Mn valence states in mixed-valent manganates by XANES spectroscopy. *American Mineralogist* **2012,** *97*, (5-6), 816-827.
65. Alfeld, M.; Wahabzada, M.; Bauckhage, C.; Kersting, K.; van der Snickt, G.; Noble, P.; Janssens, K.; Wellenreuther, G.; Falkenberg, G., Simplex Volume Maximization (SiVM): A matrix factorization algorithm with non-negative constrains and low computing demands for the interpretation of full spectral X-ray fluorescence imaging data. *Microchem J* **2017,** *132*, 179-184.
66. Webb, S. M. *SMAK: Sam's Microprobe Analysis Kit*, 0.46; Stanford Synchrotron Radiation Laboratory: Stanford, CA, 2006.
67. Ravel, B.; Newville, M., ATHENA, ARTEMIS, HEPHAESTUS: data analysis for X-ray absorption spectroscopy using IFEFFIT. *J Synchrotron Radiat* **2005,** *12*, (Pt 4), 537-41.
68. Webb, S. M., SIXPack a Graphical User Interface for XAS Analysis Using IFEFFIT. *Physica Scripta* **2005**, 1011.
69. Gilkes, R. J.; McKenzie, R. M., Geochemistry of manganese in soil. In *Manganese in soils and plants*, R.D., G.; R.J., H.; N.C., U., Eds. Kluwer Academic Publishers: 1988; pp 23-37.
70. Madison, A. S.; Tebo, B. M.; Mucci, A.; Sundby, B.; Luther, G. W., Abundant Porewater Mn(III) Is a Major Component of the Sedimentary Redox System. **2013,** *341*, (6148), 875-878.
71. Schlüter, S.; Vogel, H. J., Analysis of Soil Structure Turnover with Garnet Particles and X-Ray Microtomography. *Plos One* **2016,** *11*, (7), e0159948.
72. Milliken, G. A.; Johnson, D. E., *Analysis of Messy Data Volume I: Designed Experiments*. 2nd ed.; CRC Press: 2009.

753 73. Kravchenko, A. N.; Toosi, E. R.; Guber, A. K.; Ostrom, N. E.; Yu, J.; Azeem, K.; Rivers, M. L.;
754 Robertson, G. P., Hotspots of soil N2O emission enhanced through water absorption by plant residue.
755 *Nat Geosci* **2017,** *10*, (7), 496-+.
756 74. Thompson, I. A.; Huber, D. M.; Guest, C. A.; Schulze, D. G., Fungal manganese oxidation in a
757 reduced soil. *Environ Microbiol* **2005,** *7*, (9), 1480-7.
758 75. Graham, R. D.; Quirk, J. P., An Historical Preface. In *Manganese in Soils and Plants: Proceedings*
759 *of the International Symposium on 'Manganese in Soils and Plants' held at the Waite Agricultural*
760 *Research Institute, The University of Adelaide, Glen Osmond, South Australia, August 22–26, 1988 as an*
761 *Australian Bicentennial Event*, Graham, R. D.; Hannam, R. J.; Uren, N. C., Eds. Springer Netherlands:
762 Dordrecht, 1988; pp 1-6.
763 76. Emerson, D. W.; Garen, R. E.; Ghiorse, W. C., Formation of Metallogenium-like structures by a
764 manganese-oxiding fungus. *Archives of Microbiology* **2004,** *151*, 223-231.
765 77. Otten, W.; Hall, D.; Harris, K.; Ritz, K.; Young, I. M.; Gilligan, C. A., Soil Physics, Fungal
766 Epidemiology and the Spread of Rhizoctonia solani. *The New Phytologist* **2001,** *151*, (2), 459-468.
767 78. Soufan, R.; Delaunay, Y.; Gonod, L. V.; Shor, L. M.; Garnier, P.; Otten, W.; Baveye, P. C., Pore-
768 Scale Monitoring of the Effect of Microarchitecture on Fungal Growth in a Two-Dimensional Soil-Like
769 Micromodel. **2018,** *6*.
770 79. Guest, C. A.; Schulze, D. G.; Thompson, I. A.; Huber, D. M., Correlating Manganese X-Ray
771 Absorption Near-Edge Structure Spectra with Extractable Soil Manganese. *Soil Sci Soc Am J* **2002,** *66*, (4),
772 1172-1181.
773 80. Bartlett, R. J., Manganese Redox Reactions and Organic Interactions in Soils. In *Manganese in*
774 *Soils and Plants: Proceedings of the International Symposium on 'Manganese in Soils and Plants' held at*
775 *the Waite Agricultural Research Institute, The University of Adelaide, Glen Osmond, South Australia,*
776 *August 22–26, 1988 as an Australian Bicentennial Event*, Graham, R. D.; Hannam, R. J.; Uren, N. C., Eds.
777 Springer Netherlands: Dordrecht, 1988; pp 59-73.
778 81. Santelli, C. M.; Webb, S. M.; Dohnalkova, A. C.; Hansel, C. M., Diversity of Mn oxides produced
779 by Mn(II)-oxidizing fungi. *Geochimica Et Cosmochimica Acta* **2011,** *75*, (10), 2762-2776.
780 82. Stendahl, J.; Berg, B.; Lindahl, B. D., Manganese availability is negatively associated with carbon
781 storage in northern coniferous forest humus layers. *Scientific Reports* **2017,** *7*, (1), 15487.
782 83. Grybos, M.; Davranche, M.; Gruau, G.; Petitjean, P.; Pedrot, M., Increasing pH drives organic
783 matter solubilization from wetland soils under reducing conditions. *Geoderma* **2009,** *154*, (1-2), 13-19.
784 84. Tipping, E.; Heaton, M. J., THE ADSORPTION OF AQUATIC HUMIC SUBSTANCES BY 2 OXIDES OF
785 MANGANESE. *Geochim Cosmochim Ac* **1983,** *47*, (8), 1393-1397.

786